AIMS Biophysics, 4(3): 465-490.
DOI: 10.3934/biophy.2017.3.465
Received: 28 February 2017
Accepted: 13 July 2017
Published: 18 July 2017

http://www.aimspress.com/journal/biophysics

Review

Modelling cell death for cancer hadrontherapy

Mario P. Carante [1,2] and Francesca Ballarini [1,2,*]

[1] Department of Physics, University of Pavia, via Bassi 6, I-27100 Pavia, Italy
[2] INFN-National Institute of Nuclear Physics, Section of Pavia, via Bassi 6, I-27100 Pavia, Italy

* **Correspondence:** Email: francesca.ballarini@unipv.it; Tel: +39-0382-987949.

Abstract: Many cancer types are treated more and more frequently with protons or Carbon ions, which allow obtaining a high dose conformation to the tumor and, in the case of Carbon, a high biological effectiveness, which makes heavy ions particularly suitable to treat tumors that are resistant to conventional photon therapy. For Carbon ions it is therefore mandatory an evaluation of the beam biological effectiveness, which depends not only on the particle energy, and thus the depth in tissue, but also on many other parameters including dose, cell type and considered biological effect. In specific cases, typically for single-field irradiation of tumors located immediately before an organ at risk, this kind of evaluation may be useful also for protons, for which the constant biological effectiveness currently assumed in clinics may be sub-optimal. In principle such evaluation can be based both on experimental data and on biophysical models; of course, both methods have advantages and drawbacks. In this framework, the two main approaches adopted for Carbon therapy, that is the Local Effect Model (LEM) used in Germany and Italy and the empirical approach used in Japan, will presented and discussed, as well as an alternative model called Microdosimetric-Kinetic Model (MKM). Some recent phenomenological models specific for protons, which share as a common basis the so-called Linear-Quadratic formulation, will also be reviewed. Finally, a biophysical model of cell death and chromosome aberrations called BIANCA (BIophysical ANalysis of Cell death and chromosome Aberrations), developed in Pavia (Italy), will be presented.

Keywords: hadrontherapy; cell death; chromosome aberrations; biophysical models; Monte Carlo simulations

1. Introduction

Radiotherapy, mainly using X-rays, is one of the main treatment options in oncology and is

administered to about 50% of the patients with localized malignant tumors [1]. The idea of using charged particles instead of photons is mainly addressed to maximizing the tumor control probability while sparing normal tissues, thus limiting toxicity and side effects. Although the number of patients treated with ions is still small if compared to the total, this practice, known as hadron therapy, is rapidly diffusing worldwide. More than 60 facilities are currently in operation and more than 50 are under construction or in a planning stage; moreover, more than 150,000 patients have been treated till now [2]. The use of protons and carbon ions, and possibly other charged particles [3], has a strong rationale, mainly based on their physical properties. Their depth-dose profile, culminating with a sharp decrease beyond the Bragg peak (especially for protons), and the high collimation of ions along their path through tissues, allow for a high conformity to the tumor [4,5,6]. However, also the biological effectiveness of these particles needs to be taken into account. In particular, while protons have a similar biological effectiveness compared to photons, except for those in the distal part of the SOBP (Spread Out Bragg Peak), carbon ions have a highly non-constant depth profile of RBE (Relative Biological Effectiveness). In the latter case, along the entrance channel the LET values are lower than 20 keV/μm and the RBE is around 1, while only in the last few cm (about 4 in the case of a 26-cm-range beam) the LET reaches values around 100 keV/μm and the RBE becomes higher and higher in the tumor region.

Beam delivery and dose distribution into the patient are established through a process called treatment planning, which has the aim of ”balancing” high dose conformation to the target while sparing healthy tissues. Thanks to imaging techniques the Clinical Target Volume (CTV) and Organs At Risk (OAR) are delineated, and afterwards the maximum doses to the tumor and to healthy tissues are established. Moreover a Planning Treatment Volume (PTV) is defined, in order to take into account any geometrical variation during the therapy and all possible physical uncertainties. Then the beam directions are selected and the dose optimization is performed. The absorbed dose is calculated by a Treatment Planning System (TPS) on the basis of CT data, which provide the X-ray absorption coefficient at each location in the patient. The total dose is then calculated as a superposition of several Bragg Peaks [7]. However the purpose is not just to deliver a high dose in the tumor and a low dose in healthy tissues (and thus to produce a constant dose level along the SOBP), but more generally to have a conformity regarding the biological effectiveness. This is quantified by the product of absorbed dose and RBE, which is expressed in GyE. The integration of a RBE model into treatment planning, especially for heavy ions, is therefore essential.

A Treatment Planning System (in the case of clinical applications) or a radiation transport code like FLUKA [8], PHITS [9] or GEANT4 [10] (mainly used for research purposes or plan validation), providing the dose distribution in the patient, need therefore to be coupled with a biophysical model. The two main models currently used worldwide for carbon-ion therapy are the Local Effect Model (LEM), developed at GSI in Germany [11], and the Microdosimetric-Kinetic Model (MKM), used in Japan [12]. These two approaches will be described in the first part of this review. Concerning protons, however, radiobiological models are not commonly included into Treatment Planning Systems, and a constant RBE value of 1.1 is generally assumed along the whole SOBP. Nevertheless there are many experimental studies, basing on both *in vitro* and *in vivo* irradiation, indicating that this is only an approximation since proton RBE depends on several factors, such as the particle type and energy, the dose level [13] and the irradiated tissue type or cell line [14]. In particular, many experimental data show that proton RBE is not constant with depth along a SOBP, but is characterized by a significant increase in the distal region, due to an excess of low energy (and thus higher LET) protons [15–18].

In vivo, the mean RBE at mid-SOBP was evaluated as ~1.1, ranging from 0.7 to 1.6; *in vitro* cell survival data indicate a mean value at mid-SOBP of ~1.2, ranging from 0.9 to 2.1. Furthermore, both *in vitro* and *in vivo* data tend to show a significant RBE increase for lower fractional doses, especially in the case of low α/β ratio. This may explain why *in vivo* experiments, many of which have been performed at higher doses, indicated lower RBE values than *in vitro* studies. A recent and extensive analysis of proton RBE experiments, which is beyond the scope of the present paper, can be found in [19], where the predictions of the Local Effect Model (LEM) were compared considering 19 publications with *in vitro* experiments and 10 publications with *in vivo* experiments.

On the other hand, the currently available results are affected by uncertainties, and it is fundamental to integrate the experimental data with theoretical approaches, in order to have information covering a wide range of conditions and values of dose, LET and radio-sensitivity. Various models exist taking into account RBE deviations from the 1.1 constant value used in clinics; these approaches will be discussed in the second part of this review. Finally, a biophysical model called BIANCA (BIophysical ANalysis of Cell death and chromosome Aberrations), developed at the University of Pavia and the INFN Section of Pavia, Italy, will be described.

2. The Local Effect Model

The Local Effect Model (LEM) is currently used for the radiobiological optimization of carbon-ion treatment planning in Germany and at CNAO in Pavia, Italy. The LEM was initially proposed by Scholz and Kraft at GSI in Darmstadt, Germany, in 1994 [11]. The basic assumption is that the local biological effect, that is the damage in a small cellular sub-volume, is determined by the expectation value of energy deposition in that sub-volume, and is independent of the radiation type. Thus, for a fixed biological target, the only difference relies on the different radiation track structures. In the model, the various particle tracks are assumed to have a radial dose distribution given by

$$D(r) = \begin{cases} \lambda LET_{\infty} \frac{1}{r_{min}^2} & r < r_{min} \\ \lambda LET_{\infty} \frac{1}{r^2} & r_{min} \le r \le r_{max} \\ 0 & r > r_{max} \end{cases} \quad (1)$$

According to [20], LET_{∞} is the unrestricted LET in water and λ is a normalization constant, which is adjusted so that the integral over the whole track yields the LET as given by the tables reported in [21] and [22].

The track core with radius r_{min} represents the region where the dose is constant. In the first model version, r_{min} had a fixed value of 10 nm, taking into account also the diffusion of free radicals. On the contrary in the third version of the model [23], the authors took into account that the extension of the track core should increase with the primary particle velocity, since the distance of the primary excitation and ionization events from the trajectory is energy-dependent. The velocity-dependent radius of the inner part of the track was thus parametrized as follows:

$$r_{min} = \beta \cdot r_c \quad (2)$$

where $\beta = v/c$, and r_c is the largest extension of the track core in the limit $v = c$. On the other hand r_{max} represents the maximum radial distance travelled by the δ-electrons with the highest energy. It is

parametrized as a function of the ion energy (*E*, expressed in *MeV/u*), according to the following empirical formula [24]:

$$r_{max} = \gamma \cdot E^{\delta} \tag{3}$$

where

$$\gamma = 0.062 \frac{\mu m}{(MeV/u)^{\delta}} \qquad \delta = 1.7 \tag{4}$$

Once the dose deposition is known, it is possible to compute the surviving probability for ion irradiation if the response of the same cell line to photons is known. The phenomenological modelization assumed for X-ray survival curves is linear-quadratic, with an exponential tail for doses exceeding a threshold D_t, as follows:

$$-lnS_X(D) = \begin{cases} \alpha_X D + \beta_X D^2 & D < D_t \\ \alpha_X D_t + \beta_X D_t^2 + s_{max}(D - D_t) & D \geq D_t \end{cases} \tag{5}$$

where $s_{max} = \alpha_X + 2\beta_X D_t$ is the slope of the exponential tail. D_t is a semi-free parameter; it is difficult to measure but, from experimental data, it is known to lie between 10 and 40 Gy.

The first step in order to calculate the survival probability for ion irradiation is the Poisson assumption for lethal events, leading to the following survival probability for X-rays:

$$S_X(D) = e^{-N_X(D)} \tag{6}$$

where N_X (D) is the mean number of lethal events per cell after D. Therefore,

$$N_X(D) = -lnS_X(D) \tag{7}$$

Since ions and photons are assumed to interact locally with the cell in the same way and the only difference relies in the dose distribution within the cell nucleus, the local effect in each sub-volume of the nucleus can be calculated by the only knowledge of the dose deposited within it, and of the X-ray survival probability for that dose level. The total dose will then be given by the sum of the contributions of all the ion tracks. The average number of lethal events induced per cell by ion irradiation can be obtained by integration of the local density *v(d(x; y; z))* for the production of lethal events (assumed to be identical for ions and photons).

$$\bar{N}_{Ion} = \int v\big(d(x,y,z)\big) dV_{Nucleus} = \int \frac{-ln(S_X(d(x,y,z)))}{V_{Nucleus}} dV_{Nucleus} \tag{8}$$

where $S_X(d)$ denotes the X-ray dose response curve. It is thus sufficient to know $S_X(d)$ and the ion dose distribution to calculate the ion surviving fraction through the relationship:

$$S_{Ion} = e^{-\bar{N}_{Ion}} \tag{9}$$

Simulations over a large number of cells are usually performed in order to obtain a reliable value for S_{ion}.

The model has been tested against several experimental data sets, such as survival curves for Chinese Hamster Ovary (CHO) cells, V79 and XRS cells exposed to carbon and oxygen mono-energetic beams, and for CHO cells exposed to a 270 MeV/u carbon Spread-Out Bragg Peak (SOBP) [25,26]. Comparisons with RBE_α experimental data for two different mammalian cell lines (V79 and CHO) were also

performed [26]. Moreover, the model predictions were tested against *in vivo* data on the tolerance of the rat spinal cord [23].

Table 1 reports comparisons between model predictions obtained by the first three LEM versions and experimental data taken from the literature. Such comparisons are based on a work reported in [23], where deviations of predicted values of RBEα (i.e., RBE for the survival curve initial slope) from experimental values were evaluated for different cell lines at two Carbon LET values (13 and 77 keV/μm, representative of the entrance channel and the Bragg peak region, respectively). While LEM I (as well as LEM II, although in a reduced fashion) underestimates the therapeutic ratio of Carbon ions (i.e. the ratio of RBE in the Bragg peak region as compared with the RBE in the entrance channel), LEM III almost completely compensates these systematic deviations.

Table 1. Comparisons of LEM predictions with experimental data. Adapted from ref. [23].

	ΔRBE_α* (13 keV/μm)	ΔRBE_α* (77 keV/μm)
LEM I	0.45 ± 0.07	–0.17 ± 0.06
LEM II	0.29 ± 0.07	–0.10 ± 0.06
LEM III	0.11 ± 0.03	–0.02 ± 0.06

* the values of ΔRBE_α reported in the table represent average deviations with respect to the various cell lines considered in [23], where the deviation for each cell line was calculated as $\Delta RBE = (RBE_{LEM} - RBE_{Exp})/RBE_{Exp.}$

Finally, in 2010 the approach was generalized by directly relating the biological response to double-strand break (DSB) patterns (LEM IV) [27]. Cell damage was assumed to depend on the local DSB density, regardless of the primary particle type. Two types of damage were distinguished: isolated DSBs (iDSBs) and clustered DSBs (cDSBs). The latter were defined as at least 2 DSBs occurring in the same cubic sub-volume with side length l_{DSB} = 540 nm, corresponding to a DNA giant loop (which consists of approximately 2 Mega-base-pairs). A complexity index was defined as follows:

$$C = \frac{N_{cDSB}}{N_{cDSB}+N_{iDSB}} \tag{10}$$

where N denotes the number of a specific damage type. The ion-induced effect was then calculated on the basis of the equivalent photon dose corresponding to the same complexity index.

This model version was validated through the comparison of simulation results with several experimental data, such as CHO survival data in a typical two-port irradiation with protons and carbon ions and after irradiation with a mono-directional 4-cm extended Bragg peak of Helium ions. Predictions were also performed on the RBE variability along different carbon SOBPs [28]. This work showed that the differences in the prediction of RBE-weighted doses and iso-effective doses between LEM I and LEM IV for typical tumor volumes (i.e. averaged over the patient population in the GSI pilot project) are less than 10%. The authors therefore concluded that the transition to LEM IV is not expected to lead to significant differences in the TCP dose-response relationship for chordoma as compared to the analysis based on LEM I.

3. The NIRS Approach

At NIRS in Chiba, Japan, the RBE is calculated by means of a method proposed by Kanai et al. [29], basing on the linear-quadratic (LQ) model. More specifically, dose-averaged values of the α and β coefficients for a mixed beam are calculated starting from the coefficients for mono-energetic beams derived from empirical tables:

$$\alpha_{mix} = \sum f_i \alpha_i \quad \sqrt{\beta_{mix}} = \sum f_i \sqrt{\beta_i} \tag{11}$$

where α_i and β_i are the parameter values for mono-energetic beams, and $f_i = d_i/D$ is the fraction of dose delivered by the i_{th} mono-energetic beam.

For patient treatment planning [30], *in vitro* human salivary gland (HSG) tumor cells were used, assuming that the moderate radio-sensitivity of this cell line is representative of a typical tumor response. The RBE for the survival of HSG cells was measured at different depths of different HIMAC SOBPs; the distributions of relative physical and biological dose obtained using HSG cells were assumed to be maintained for the various clinical cases, obtaining a nearly universal SOBP profile for different Carbon energies and different SOBP widths, which allowed obtaining a flat response for HSG survival [31]. To account for the difference between the *in vitro* and the *in vivo* response, the radiobiological RBE values were then rescaled to values of "clinical RBE", according to the RBE observed in previous clinical experience with fast neutrons. More specifically, since the neutron therapy experience indicated a neutron clinical RBE of 3.0, the clinical RBE at the neutron-equivalent position of a carbon SOBP was also determined to be 3.0. To determine the neutron-equivalent position, the RBE measurements for Carbon were compared with RBE measurements for neutrons; such comparison suggested that NIRS neutrons were biologically equivalent (in terms of HSG survival) to C-ions at a SOBP depth where the (dose-averaged) LET is ~80 keV/μm. The dose level of the flat top of the biological dose distribution was prescribed by a medical doctor, and the physical dose at the neutron-equivalent position was determined using the RBE = 3.0 assumption, that is dividing the prescribed biological dose by 3.0. Knowledge of the physical dose at the neutron-equivalent position allowed deriving the entire SOBP physical-dose distribution, which was normalized with respect to the neutron-equivalent position. In particular, this allowed obtaining the physical dose at the SOBP center, and thus the RBE at the SOBP center, which was derived by dividing the prescribed biological dose by the physical dose.

In Phase I/II trials, the prescribed dose was gradually escalated from a relatively lower level to a higher level, to seek the optimum dose level while not causing any severe complication to surrounding normal tissues. These studies allowed verifying that carbon ions could be safely and effectively used for radiotherapy [32]. Furthermore [33], a retrospective analysis of clinical results was carried out by means of TCP (tumor control probability) curves for non-small cell lung cancer, comparing the outcome to the original biophysical parameters.

4. The Microdosimetric Kinetic Model (MKM)

Another approach for predicting cell survival following ion irradiation is the Microdosimetric Kinetic Model (MKM), developed by Hawkins [34,35] basing on the Theory of Dual Radiation Action (TDRA) by Kellerer and Rossi [36]. However, while the latter assumes that a lethal lesion is

due to the association of two sub-lethal lesions, according to the former also a sub-lethal lesion that has not been repaired after a certain amount of time can lead to cell death. According to the MKM, cell killing depends on the distribution of energy imparted to a sub-nuclear region, called "domain". The mean number of lethal lesions in a domain is given by

$$L_d = Az + Bz^2 \tag{12}$$

where z is the specific energy, that is the ratio between the energy imparted in the domain and the domain mass. Assuming a Poisson distribution of lethal lesions among the cells, the mean number of lethal lesions in the nucleus, L (which is related to the surviving fraction S by the relationship S = exp(-L)), can be expressed as follows:

$$L = N < L_d >= (\alpha_0 + \beta z_{1D})D + \beta D^2 \tag{13}$$

where N is the number of domains in the nucleus, D is the radiation dose, α_0 is the slope in the limit LET = 0, β is assumed to be independent of radiation quality, and z_{1D} is the dose-mean specific energy by single energy deposition in a domain, taking into account that $<z^2> = (z_{1D}D + D^2)$. Modelling the nucleus as a cylinder of radius R composed by a certain number of domains of radius r, z_{1D} can be expressed as:

$$z_{1D} = \frac{ly_D}{m} = \frac{y_D}{\rho\pi r^2} \tag{14}$$

where m, ρ and l are the mass, density and mean chord length of the domain, respectively, and y_D is the domain "lineal energy", defined as the ratio between the energy imparted for a single event and the domain mean chord length.

To account for the so-called "over-killing effect", Kase et al. [12] replaced z_{1D} by $z_{1D}^* = ly^*/m$, where y* was calculated from the probability density of y, f(y), and a coefficient called y_0. More specifically:

$$y^* = y_0^2 \frac{\int[1-exp(-y^2/y_0^2)]f(y)dy}{\int yf(y)dy} \tag{15}$$

When the y spectrum was a δ function, y_0 could be calculated by

$$y_0 = \frac{\rho\pi r R^2}{\sqrt{\beta(r^2+R^2)}} \tag{16}$$

Denoting by α the quantity $(\alpha_0 + \beta z_{1D}^*)$ and calling D_x the photon dose (considering photons as a reference radiation) to obtain S, the radiobiological RBE can thus be written as follows:

$$RBE = \frac{2\beta D_x}{-\alpha+\sqrt{\alpha^2-4\beta\, ln\, S}} \tag{17}$$

Apart from β, which is determined by the photon response since it is assumed to be independent of radiation quality, the parameters of the model are thus α_0 (slope of the survival curve in the limit LET = 0), r (domain radius) and R (nucleus radius). Using amorphous track-structure models for the MKM calculations, the same group of authors [37] showed that the MKM approach can predict *in vitro* cell survival for mono-energetic ^{12}C beams, as well as ^{3}He and ^{20}Ne.

Subsequently, Inaniwa et al. [38] developed a method to calculate the RBE of mixed fields

based on the modified MKM, and integrated the modified MKM into a research version of a treatment planning system. D_{10} values calculated for different combinations of the three model parameters were compared with published D_{10} data of *in vitro* HSG cells exposed to mono-energetic ^{3}He-, ^{12}C- or ^{20}Ne-ions [39], leading to R = 3.9 μm, r = 0.32 μm and $\alpha_0 = 0.172$ Gy^{-1} following best fit. This allowed producing a table with z_{1D}* values for many different mono-energetic ions. The z_{1D}* value for a scanned carbon beam at a given position was then derived by "weighting" the various z_{1D}* values delivered by the different beams at that position (provided by Monte Carlo simulations based on Geant4) by the corresponding doses and beam intensities. The method was then integrated into the research version of a treatment planning system [40]. To verify the method, HSG cell survival irradiation experiments were performed at different depths for a scanned carbon beam. Good agreement was found between the predicted and observed cell survival, as well as the planned and measured dose distributions.

In addition to the aforementioned works, further modifications were performed, leading to new MKM versions that were applied to the estimation of cell survival for both targeted and non-targeted effects [41,42,43].

Comparisons between cell survival calculations performed by the LEM or the MKM approach can be found in [37], where amorphous track-structure models—instead of stochastic models—were used for MKM calculations, finding that such calculations can predict mammalian cell survival curves for He-3, C-12 and Ne-20 beams. Cell survival calculations were also performed by two different implementations of LEM, which is inherently based on an amorphous track-structure model, finding good agreement with the considered experimental data. In the context of the amorphous track-structure model, the differences between LEM and MKM were mainly ascribed to different approaches in calculating the biological effects of the very high local dose delivered in the center of ion tracks. A direct comparison between cell survival calculations performed by LEM (using the LEM-oriented track-structure model) or MKM (using the Kiefer-Chatterjee model) for Carbon-irradiated CHO cells can be found in figure 13 of the original paper, which reports 1%, 10% and 50% survival doses as a function of LET calculated by MKM or two different LEM versions, compared to experimental data. According to the authors, MKM calculations were found to reflect the 1%, 10% and 50% survival doses, and LEM calculations showed reasonably good agreement with the considered experimental data for all considered LET values except 100 and 150 keV/μm. These two LET values showed a relatively large mismatch at 10% and 1% survival, respectively, which was partly compensated by the modified LEM. However, for other cell lines such as HSG cells, and according to other experiments more closely related to cancer therapy [44], the agreement of high-LET particles representative of the SOBP with experimental data was much better, although the effectiveness of low-LET particles was overestimated to some extent.

Other comparisons between LEM and MKM can be found in [45], which describes the coupling of the NIRS clinical dose to the FLUKA Monte Carlo code. A high level of agreement was found with published data by exploring a range of values for the MKM input parameters, whereas some differences were found in forward recalculations of NIRS patient plans, mainly attributable to differences with the analytical TPS dose engine in describing the mixed radiation field. In addition to the NIRS approach, LEM-I and LEM-IV RBE tables (both related to $\alpha/\beta = 2$ Gy) were used, allowing to compare profiles of effective dose and RBE for a prostate cancer as computed by the NIRS approach, LEM-I or LEM-IV coupled with FLUKA. Such comparisons, which can be found in figure 5 of the original paper, showed that both LEM-I and LEM-IV effective-dose profiles reached a

similar dose level at the target center, in the middle of the modulated region. LEM-IV-based calculations showed a pronounced peak at the distal end of the SOBP if compared with LEM-I. Furthermore, RBE values based on LEM-IV and NIRS already matched in the SOBP region, whereas RBE values based on LEM-I were 64% higher than those based on the NIRS approach. More generally, this work showed that Monte Carlo tools can provide an important contribution in model inter-comparison.

5. Proton-specific Approaches

5.1. Model description

Unlike the case of carbon therapy, biophysical models are not currently implemented in proton therapy treatment planning systems. However, to take into account the possible variations of proton RBE, different theoretical approaches may be applied to the proton case, such as the previously described LEM and MKM and the repair-misrepair-fixation (RMF) model [46]. Recently, various phenomenological models specific for protons have also been proposed. The starting point of all these approaches is the Linear-Quadratic (LQ) formulation, according to which the general dependence of the surviving fraction on the absorbed dose D is given by

$$S = e^{-(\alpha D+\beta D^2)} \tag{18}$$

where α and β are two parameters. According to this approach, a given proton dose (D_p) will produce the same effect of a given dose of a reference radiation (D_x in the case of X-rays) if the following condition is satisfied:

$$\alpha_x D_x + \beta_x D_x^2 = \alpha_p D_p + \beta_p D_p^2 \tag{19}$$

where the index p denotes proton irradiation and the index x denotes photon irradiation. To obtain an expression for the explicit dependence of RBE on the photon dose and the cell-specific ratio α_x/β_x, equation (19) can be divided by D_x and β_x, thus obtaining

$$\left(\frac{\alpha_x}{\beta_x} + D_x\right) RBE^2 - \frac{\alpha_p}{\beta_x} RBE - \frac{\beta_p}{\beta_x} D_x = 0 \tag{20}$$

where the definition of RBE, which is the ratio between the photon and proton dose to obtain the same effect, has been applied. By solving this equation, and by pointing out the role of α_x/β_x, we obtain

$$RBE = \frac{\frac{\alpha_x \alpha_p}{\beta_x \alpha_x} + \sqrt{\left(\frac{\alpha_x}{\beta_x}\right)^2 \left(\frac{\alpha_p}{\alpha_x}\right)^2 + 4\frac{\alpha_x \beta_p}{\beta_x \beta_x} D_x + 4\frac{\beta_p}{\beta_x} D_x^2}}{2\left(\frac{\alpha_x}{\beta_x} + D_x\right)} \tag{21}$$

Equivalently, to make explicit the dependence of RBE on the proton dose and the α_x/β_x ratio, equation (19) can be divided by D_p^2, thus obtaining the following expression

$$RBE = \frac{-\frac{\alpha_x}{\beta_x} + \sqrt{\left(\frac{\alpha_x}{\beta_x}\right)^2 + 4\frac{\alpha_x \alpha_p}{\beta_x \alpha_x} D_p + 4\frac{\beta_p}{\beta_x} D_p^2}}{2D_p} \tag{22}$$

It is now convenient to introduce the two quantities RBE_{max} and RBE_{min}, which represent the asymptotic values of RBE in the limit of 0 and ∞ dose, respectively: in the limit 0 dose, the quadratic terms of Equation (1) can be neglected, leading to $\alpha_x D_x = \alpha_p D_p$, and thus

$$RBE_{max} = \frac{\alpha_p}{\alpha_x} \tag{23}$$

On the contrary, in the limit of ∞ dose, one can neglect the linear terms, leading to $\beta_x D_x^2 = \beta_p D_p^2$, and thus

$$RBE_{min} = \sqrt{\frac{\beta_p}{\beta_x}} \tag{24}$$

Equations (21) and (22) thus become

$$RBE = \frac{\frac{\alpha_x}{\beta_x} RBE_{max} + \sqrt{\left(\frac{\alpha_x}{\beta_x}\right)^2 RBE_{max}^2 + 4\frac{\alpha_x}{\beta_x} RBE_{min}^2 D_x + 4RBE_{min}^2 D_x^2}}{2\left(\frac{\alpha_x}{\beta_x} + D_x\right)} \tag{25}$$

and

$$RBE = \frac{-\frac{\alpha_x}{\beta_x} + \sqrt{\left(\frac{\alpha_x}{\beta_x}\right)^2 + 4\frac{\alpha_x}{\beta_x} RBE_{max} D_p + 4RBE_{min}^2 D_p^2}}{2D_p} \tag{26}$$

respectively.

At this level, the various phenomenological models differ in the assumed dependence of RBE_{max} and RBE_{min} on the radiation LET and on the tissue type (that is, on α_x/β_x), and on the experimental data used to obtain these dependences.

For example, the approach of Tilly et al. [47], based on experimental data by Belli et al. [48,49,50], Folkard et al. [51] and Bettega et al. [52] regarding different cell lines over a wide LET range, assumed a linear dependence of RBE_{max} on LET, with a slope depending on the α_x/β_x ratio. In particular, the data were divided into two groups (with $\alpha_x/\beta_x \sim 2$ and ~10, respectively) and fitted separately. The β value was found to be almost constant up to a LET value of about 30 keV/μm. Another similar approach is that of Frese et al. [53], who started from the same ideas of a previous work [54] assuming a linear dependence of α on dose-average LET, as follows:

$$\alpha_p = \alpha_0 + \lambda \cdot LET \tag{27}$$

Here α_0 is a normalization parameter representing the initial value of α_p, which should be equal to α_x.

It was thus assumed that

$$\alpha_0 = \alpha_x - 0.5 keV/\mu m \cdot \lambda \tag{28}$$

where 0.5 keV/μm represents the LET value in the entrance channel of a clinical proton beam, according to ICRU report 49 [55]. A single λ value for all tissues was derived by imposing a similar

mean RBE value in the target with respect to treatment plans based on a fixed RBE of 1.1. Basing on the treatment plans of four patients, an average λ value of 0.008 μm/(keV·Gy) was found. Concerning the β_p parameter, it was considered constant and equal to β_x. The expression for RBE thus becomes:

$$RBE = \frac{-\frac{\alpha_x}{\beta_x} + \sqrt{\left(\frac{\alpha_x}{\beta_x}\right)^2 + 4\frac{\alpha_x}{\beta_x}\left(1 + \frac{\lambda}{\alpha_x}(LET - 0.5keV/\mu m)\right)D_p + 4D_p^2}}{2D_p} \tag{29}$$

A different approach was adopted by Carabe et al. [56], who assumed for both RBE_{max} and RBE_{min}, that is for both α_p and β_p, a linear dependence on LET and an inverse dependence on the tissue-specific parameter α_x/β_x. The resulting expressions were:

$$RBE_{max} = 0.843 + 0.154\frac{2.686}{\left(\alpha_x/\beta_x\right)}LET \tag{30}$$

and

$$RBE_{min} = 1.09 + 0.006\frac{2.686}{\left(\alpha_x/\beta_x\right)}LET \tag{31}$$

The numerical parameters were obtained by fitting experimental data [13,48,51,57,58,59] relating RBE and LET for V79 cells. The value 2.686 represents the average α_x/β_x resulting from the experiments. Wedenberg et al. [60] assumed a similar behaviour for RBE_{max}, described by the following equation:

$$RBE_{max} = 1 + \frac{qLET}{\left(\alpha_x/\beta_x\right)} \tag{32}$$

This equation holds for LET values lower than 30 keV/μm. RBE_{min}, on the contrary, was assumed to be constant and equal to 1. The best value for the q parameter was found to be 0.434 Gy/(keV/μm). This value, as well as the qualitative behaviours of α_p and β_p, was obtained by statistical analyses of experimental data of 10 different cell lines, irradiated with near mono-energetic proton beams with LET values ranging from 6 to 30 keV/μm. The resulting expression for RBE was

$$RBE = \frac{-\frac{\alpha_x}{\beta_x} + \sqrt{\left(\frac{\alpha_x}{\beta_x}\right)^2 + 4\left(\frac{\alpha_x}{\beta_x} + qLET\right)D_p + 4D_p^2}}{2D_p} \tag{33}$$

A wider experimental data set was used by Paganetti [61], with 76 literature papers on cell survival considered. The RBE was linearly fitted as a function of LET, that is

$$RBE = A \cdot LET + B \tag{34}$$

The fit was performed for four different bins of α_x/β_x (specifically: $\alpha_x/\beta_x < 3$ Gy; 3 Gy $\leq \alpha_x/\beta_x <$ 6 Gy; 6 Gy $\leq \alpha_x/\beta_x < 9$ Gy; $\alpha_x/\beta_x \geq 9$ Gy) and for two different proton doses (2 and 6 Gy). Only data for LET < 15 keV/μm were chosen. The author found a positive slope, which decreased with increasing dose. The slopes were similar for all the α_x/β_x regions. Concerning the dependence of RBE on α_x/β_x, the data were linearly fitted for four different LET bins (specifically: LET < 3 keV/μm; 3 keV/μm ≤ LET < 6 keV/μm; 6 keV/μm ≤ LET < 9 keV/μm; 9 keV/μm ≤ LET ≤ 15 keV/μm), two

different dose levels (2 and 6 Gy), and for $\alpha_x/\beta_x < 20$ Gy. Unexpectedly, the results do not fully confirm the theoretical prediction of a RBE increase with decreasing α_x/β_x, with some negative and some positive slopes. Finally, RBE_{max} and RBE_{min} as a function of LET were fitted by linear functions; the former showed a positive slope decreasing with increasing α_x/β_x, whereas values around zero were found for the slope of the latter.

The comprehensive collection of data in [61] was exploited to develop a new phenomenological model aimed to explicitly parametrize the dependence of RBE on dose, LET and α_x/β_x. [62]. Only data points with LET < 20 keV/μm and $\alpha_x/\beta_x < 30$ Gy were considered. The main assumptions of the model were the dependence of RBE_{max} on LET and on the inverse of α_x/β_x (like in the models by Carabe and Wedenberg), and the dependence of RBE_{min} on LET and on $\sqrt{\alpha_x/\beta_x}$, as follows:

$$RBE_{max} = p_0 + \frac{p_1}{\left(\alpha_x/\beta_x\right)} LET \tag{35}$$

$$RBE_{min} = p_2 + p_3\sqrt{\left(\frac{\alpha_x}{\beta_x}\right)} LET \tag{36}$$

where $p_{0\text{-}3}$ are the fit parameters of the model. The expression for RBE can be deduced by modifying Equation (26) according to (35) and (36). After fitting the experimental data, the parameter values were found to be $p_0 \approx 0.991$, $p_1 \approx 0.356$, $p_2 \approx 1.101$, $p_3 \approx -0.004$, with their associated uncertainties. The resulting expression for RBE is thus

$$RBE = \frac{-\frac{\alpha_x}{\beta_x} + \sqrt{\left(\frac{\alpha_x}{\beta_x}\right)^2 + 4\frac{\alpha_x}{\beta_x}\left(0.991 + \frac{0.356}{\left(\alpha_x/\beta_x\right)} LET\right) D_p + 4\left(1.101 - 0.004\sqrt{\left(\frac{\alpha_x}{\beta_x}\right)} LET\right)^2 D_p^2}}{2D_p} \tag{37}$$

According to the model, RBE increases with increasing LET, and decreases with increasing dose and α_x/β_x ratio.

5.2. Model applications

Although these models are not currently integrated into treatment plans routinely used in clinics, their authors investigated the consequences of applying a constant RBE instead of taking into account its variations. For instance, Tilly et al. [47] applied their study to a clinical case of advanced hypopharynx cancer: when applying a variable RBE, its value was found to be higher both in the tumour region and in the spinal cord, an organ at risk, compared to the 1.1 constant value. However, the NTCP (Normal Tissue Complication Probability) for the spinal cord came out to be still zero. Nevertheless, the NTCP for the other normal tissues outside the CTV (Clinical Tumour Volume) was much higher with respect to the constant RBE case. The authors concluded that it is worth considering RBE variations in clinical proton therapy planning, especially when organs at risk are located immediately behind the tumour region.

Frese et al. [53] performed a study on four patients with nasopharyngeal carcinoma, previously treated with intensity-modulated radiotherapy at the German Cancer Research Center (Heidelberg, Germany). For each patient an IMPT (Intensity Modulated Protontherapy Therapy) plan was calculated assuming RBE = 1.1. By keeping the same dose, a variable RBE was then applied, as computed by their phenomenological model in agreement with Equation (29). Finally, a biologically optimized plan

was calculated, in order to obtain a treatment plan having at least the same quality as the physically optimized plan. They observed important RBE variations in the treated volumes, when calculating it with the model; moreover, when performing the biological optimization, a higher inhomogeneity in the dose distributions was obtained, due to LET variations within the volumes. Nevertheless, a biological optimization of IMPT plans was found to be possible, since the optimizations in the four considered cases led to plans of at least as good quality as physically optimized plans. Moreover, the authors highlighted how "radio-resistant normal tissues have a higher risk of overdosage than radio-sensitive tissues".

Carabe et al. [56] investigated the differences in the use of a variable or a constant RBE in terms of biological range shifts, by studying the Dose-Volume Histograms (DVH) for the case of a patient with an adenoid cystic carcinoma (ACC) in the lachrymal gland. In this specific case the tumour was surrounded by normal tissues with low α_x/β_x. The largest differences between the constant and variable RBE cases were observed in the case of low α_x/β_x volumes receiving low dose. In the opposite case of large doses and large values of α_x/β_x, variable RBE values even smaller of 1.1 were observed. Moreover, the biological doses in the low α_x/β_x organs at risks (optic nerve, chiasm and brainstem) were higher for the variable RBE case. Finally, since the uncertainty in the range of the biological dose profile is smaller at higher doses, the authors observed that hypo-fractionated treatment plans may allow for a reduction of the overall range uncertainty.

Wedenberg et al. [60] pointed out that late-responding tissues (low α_x/β_x) are more sensitive to LET changes than early-responding tissues (high α_x/β_x). Moreover, since the highest RBE values, in agreement with Equation (33), are expected for low α_x/β_x, high LET and low dose per fraction, particular attention should be devoted to late-responding normal tissues positioned just behind tumours and to the lateral peripheral parts of the beam, where these conditions may be satisfied. In a subsequent work [63] the authors applied their model to three brain tumour cases, by comparing a photon IMRT (Intensity-Modulated Radiation Therapy) plan, a IMPT plan with RBE = 1.1 and another proton plan with the same dose distribution but with variable RBE. When using a constant RBE value, the proton plans showed higher doses to the tumour and lower doses to the normal tissues, as compared to the photon plans. However, when the variable RBE was taken into account, the proton dose to the tumour was generally lower than the photon dose, and hot spots were found in the organs at risk (such as in the optic nerve). The authors also evaluated NTCP for some different endpoints (such as blindness and necrosis in the brain stem): the general tendency was to obtain a lower probability for constant RBE proton plans than for photon plans, but a significantly higher probability for variable RBE proton plans than for both the other cases. Such evaluation was performed for three brain tumor cases; as an example, table 2 reports NTCP estimates, in percent, for three regions of interest (R.o.I.) for case 1. In conclusion, the results indicated that the use of a constant RBE may produce sub-optimal proton treatment plans.

According to [61], the assumption of a constant RBE value of 1.1 at 2 Gy is not unreasonable, since they found an average value of 1.15 in the centre of a typical SOBP. However, caution is needed "for small modulation widths and/or low α_x/β_x, where the average RBE could be higher". Moreover, RBE was found to increase with depth up to typical average values of ~1.7 in the distal fall-off. In general, a trend of a RBE increase with decreasing α_x/β_x and with decreasing dose was observed. Finally, the authors performed a study on endpoints different from cell survival, concluding that experimental NTCP values are not sufficient to define a clear RBE behaviour, and that they are not in disagreement with a general value of 1.1, although the selected endpoints showed

important deviations from that value.

Table 2. NTCP estimates (in percent) for a brain tumour case, comparing three different plans: IMRT photons, protons with constant RBE and protons with variable RBE. Adapted from [63].

R. o. I.	Photon	constant RBE	variable RBE
Brain stem	0.84	0.57	2.13
Optic chiasm	0.88	0.18	0.91
Optic nerve	1.21	1.13	4.21

McNamara et al. [62] performed an interesting comparison between their model and the models by Carabe and by Wedenberg, applying them to the case of a SOBP with a modulation width of 10 cm and a range of 25 cm. The dose-average LET in the middle of the plateau region of the SOBP (depth: ~160–220 mm) ranged from ~1.4 to ~3.1 keV/μm, and from ~1.4 to ~10 keV/μm over the entire plateau region. Tissues with a different radio-sensitivity (α_x/β_x = 1 Gy, α_x/β_x = 2 Gy and α_x/β_x = 10 Gy) were considered. The McNamara and Wedenberg models predicted very similar results, whereas the Carabe model showed some discrepancies. However, each considered RBE model, with only slight differences, predicted an increase in biological dose at the distal edge of the SOBP. According to the McNamara model, for the case of low α_x/β_x ratio, this increase was of about 30% compared to the biological dose used in clinics (RBE = 1.1), which is a much higher value than for the case of high α_x/β_x (about 4%). In the same work, the authors also simulated two different proton treatment plans, a prostate and a paediatric head-and-neck case. They were two opposite situations: for the first case the prostate α_x/β_x value was ~1.5 Gy and the rectum and the surrounding tissue α_x/β_x was ~3.1 Gy, whereas for the second case the target volume α_x/β_x was ~11 Gy and the α_x/β_x of the rest of the brain was ~2.1 Gy. In both cases, the total prescribed dose was 1.8 Gy per fraction. In the case of the prostate treatment plan, the RBE calculated within the target was ~1.2, whereas that calculated just outside the target region was 1.3. This trend was even amplified in the head-and-neck treatment plan case, for which the RBE values within the target were ~1.1, whereas those calculated just outside the target volume, in the brainstem (which is a critical structure), were ~1.5. These studies may also have an impact on the comparison between proton and photon therapy in terms of tumour control and toxicities.

Another model inter-comparison was performed by Giovannini et al. [64], who compared the predictions of LEM-IV [27] and the approaches proposed by Carabe et al. [56] and Wedenberg et al. [60], in the framework of a variable versus constant RBE. Using the considered models, a proton SOBP and two exemplary clinical cases for cranial proton irradiation, all delivered with pencil-beam scanning, were analyzed in terms of absorbed dose, dose-averaged LET (LET_D), RBE-weighted dose (D_{RBE}), and shift of biological range. A detailed analysis, which is beyond the scope of the present work, can be found in the original paper, including the figures and tables therein reported. Herein, it is worth reporting that: (1) comparison of the RBE predictions showed different levels of agreement depending on the values of $(\alpha/\beta)_X$ and LET; (2) the SOBP study emphasized the variation of LET_D and RBE not only as a function of depth but also of the lateral distance from the central beam axis; (3) application to clinical-like scenario showed consistent discrepancies from the values obtained assuming a constant RBE of 1.1, when using a variable RBE scheme for proton irradiation in tissues with low $(\alpha/\beta)x$ (regardless of

the model); (4) shifts of biological range of 0.6–2.4 mm (for high (α/β)x) and 3.0–5.4 mm (for low (α/β)x) were found from the fall-off analysis of individual profiles of RBE-weighted fraction dose along the beam penetration depth. Concerning issue (1), Table 3 reports the resulting minimum RBE (minRBE), maximum RBE (maxRBE) and mean RBE (meanRBE) values in the PTV for one of the two patient cases analysed in [64], calculated either by LEM-IV (for two different values of the threshold dose, i.e. Dt = 10 Gy and Dt = 40 Gy), or by the Wedenberg (WED) or Carabe (CAR) models. The results are shown both for $(\alpha/\beta)_X$ = 2 Gy and for $(\alpha/\beta)_X$ = 10 Gy except for the Carabe model, which was considered as not applicable for $(\alpha/\beta)_X$ = 10 Gy [64]. Table 4 reports analogous results in terms of shift of biological range (issue 4) above. More specifically, the biological range shift (in mm) calculated by the various models in correspondence of three different dose values beyond the dose fall off (corresponding to 90% D_{presc}, 80% D_{presc} and 50% D_{presc}, respectively) are reported. Analogous to Table 3, the results are shown both for $(\alpha/\beta)_X$ = 2 Gy and for $(\alpha/\beta)_X$ = 10 Gy except for the Carabe model, which was considered as not applicable for $(\alpha/\beta)_X$ = 10 Gy.

Table 3. Minimum, maximum and mean RBE in the PTV for $(\alpha/\beta)_X$ = 2 Gy and $(\alpha/\beta)_X$ = 10 Gy for the first patient case analysed in [64] (adapted from ref. [64]).

	$(\alpha/\beta)_X$ =2 Gy			$(\alpha/\beta)_X$ =10 Gy		
Model	minRBE	maxRBE	meanRBE	minRBE	maxRBE	meanRBE
LEM D_t=10 Gy	1.10	1.70	1.19	1.05	1.34	1.09
LEM D_t=40 Gy	1.15	1.90	1.27	1.05	1.45	1.12
WED	1.20	1.64	1.24	1.10	1.26	1.11
CAR	1.20	1.60	1.27			

Table 4. Mean shift of biological range (in mm) for $(\alpha/\beta)_X$ = 2 Gy and $(\alpha/\beta)_X$ = 10 Gy for the first patient case analysed in [64] (adapted from ref. [64]).

	$(\alpha/\beta)_X$ =2 Gy			$(\alpha/\beta)_X$ =10 Gy		
Model	90% D_{presc}	80% D_{presc}	50% D_{presc}	90% D_{presc}	80% D_{presc}	50% D_{presc}
LEM D_t=10 Gy	3.74	4.33	4.07	1.73	1.81	1.64
LEM D_t=40 Gy	4.75	5.42	4.97	2.30	2.44	2.10
WED	3.16	3.64	3.39	1.11	1.16	1.03
CAR	3.10	3.51	3.17			

From this analysis the authors concluded that, although more experimental evidence is needed to validate the accuracy of the investigated models and their input parameters, their main RBE dependencies (dose, LET and (α/β)x) should be included in treatment planning. As a first step, simpler models based on the linear-quadratic formalism and LET_D might already be sufficient to reproduce important RBE dependencies for re-evaluation of plans optimized with the current RBE = 1.1 approximation.

6. The BIANCA Approach

The model presented in this section [65–72] deals both with light ions like protons and with heavier ions, including not only Carbon but also Iron, which is of great interest for space research [73–76]. The

model, called BIANCA (BIophysical ANalysis of Cell death and chromosome Aberrations), takes into account some fundamental features of the processes leading from energy deposition by radiation to DNA/chromosome damage and cell death, but at the same time requires two adjustable parameters only. According to this approach, the cell survival probability after a dose D is directly calculated from the yields of specific chromosome aberration types (dicentrics, rings and deletions, see below). In turn, chromosome aberrations are assumed to derive from mis-rejoining, or un-rejoining, of chromosome fragments, which are produced by DNA "Cluster Lesions" (CL). More specifically, the following basic assumptions are adopted:

(1) ionizing radiation induces DNA "cluster lesions", defined as DNA breaks that are severe enough to produce two independent chromosome free-ends;

(2) each free-end either remains un-rejoined (which occurs with probability f), or can be rejoined with another free-end, provided that the initial distance from the "partner" is smaller than a threshold d;

(3) dicentrics, rings and large deletions (where "large" means visible in metaphase, see below) lead to clonogenic cell death.

Since the critical DNA lesion(s) leading to important endpoints like chromosome aberrations and cell death have not been fully characterized yet, the mean number of CLs per unit dose and per unit DNA mass (mean number of CLs per Gy and per Dalton, which can be easily converted into CLs per Gy and per cell) was left as an adjustable parameter. Such parameter mainly depends on radiation quality, basically particle type and energy, and thus LET. Unless the LET is so high to be in the so-called "over-killing" region, for a given particle type the CL yield was found to increase with LET; furthermore, at a given LET, there was a tendency for lighter particles to induce more CLs than heavier particles of the same LET. The CL yield was also found to be modulated by the target cell features: more radio-resistant cells showed lower CL yields, whereas more radiosensitive cells showed higher CL yields.

Assumption (2), according to which each chromosome fragment has a certain probability of remaining un-rejoined, was recently introduced to account for the so-called "incomplete" chromosome exchanges [77]. This un-rejoining probability is likely to vary with the considered cell line, consistent with the observation that more radiosensitive cells tend to show higher frequencies of deletions [78]. Concerning a possible dependence of the un-rejoining probability on radiation quality, contradicting results are available in the literature: while in some works the percentage of incomplete exchanges was found to increase with LET [77], other studies failed to reveal such a LET-dependence [79]. Therefore, as a starting point, the value of f was assumed to be cell-line dependent but radiation-quality independent. Concerning the threshold distance for chromosome-fragment rejoining, in the most recent model version (called BIANCA II) it was set equal to the mean distance between two adjacent chromosome territories, since the occurrence of aberrations involving chromosomes located far apart in the cell nucleus is unlikely, although not impossible. Of course this distance depends on the shape and dimensions of the cell nucleus, as well as the total number of chromosomes. For instance, d was found to be ~1.6 μm for human lymphocytes (modelled as spheres with 3.0-μm radius), and ~3.0 μm for AG1522 human fibroblasts (modelled as 4.0-μm-height cylinders with elliptical base having major and minor axes of 20 and 10 μm, respectively). This approach allowed to reproduce very well yields, distributions and ratios of inter-chromosome and inter-arm exchanges (typically dicentrics and centric rings), as well as total deletion yields, although interstitial deletions were underestimated and terminal deletions

were overestimated. This suggests that representing the distance-dependence of chromosome fragment rejoining by a step function, which has similarities with the so-called "site approach" [80], allows taking into account the relationship between inter-chromosome and intra-chromosome aberrations, whereas a more detailed approach (for instance a continuously decreasing function) is necessary to account for the relationship between inter-arm and intra-arm exchanges in the same chromosome. Concerning the rejoining process, since the model applies to chromosome aberrations formed following irradiation during the G0/G1 of the cell cycle, it is assumed that repair mainly occurs via Non-Homologous End Joining (NHEJ). No distinction is made between different repair pathways, such as the so-called "canonical" or "alternative" DNA repair. Although in principle this could be done and the model would become more realistic from a biological point of view, we chose not to make this distinction to avoid introducing other free parameters in the model, which is characterized by the fact that it makes use of two adjustable parameters only.

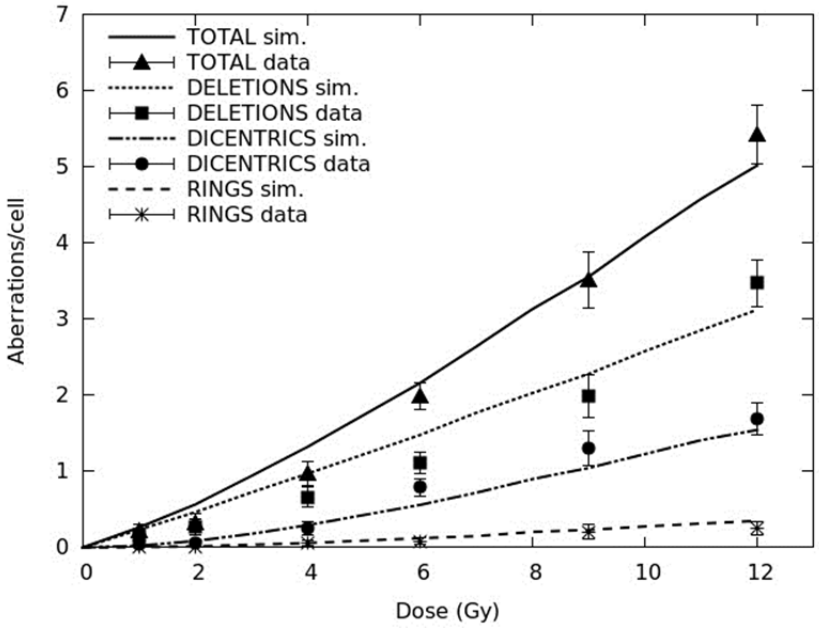

Figure 1. Yields (mean number per cell) of dicentrics, rings and deletions, as well as their sum (total aberrations) in X-irradiated AG1522 normal human fibroblasts. The lines are simulation outcomes, the points are experimental data taken from [81]. Figure taken from [71].

Examples of comparisons between simulations and data are reported in Figure 1, which shows dose-response curves for dicentrics, rings and deletions induced in X-irradiated AG1522 normal human fibroblasts. The lines are simulation outcomes, the points are experimental data taken from the literature [81]. For both dicentrics and rings, the calculated yields were within the experimental errors, with the only exception of dicentrics at 6 Gy; the capability of reproducing separately the yields of dicentrics and rings supports the assumption adopted for d, since higher d values overestimated the ratio of dicentrics to rings (the so-called "F-ratio"), whereas lower d values underestimated the F-ratio. Concerning deletions, while the simulated response is basically linear, the experimental one shows a non-negligible quadratic component. This may be explained considering

that in the simulations most deletions were "terminal deletions", which being due to a single chromosome break involve a single-particle mechanism proportional to dose, whereas most experimental deletions were of the "interstitial" type, which requiring two chromosome breaks (also) involves a two-particle mechanism proportional to the square of dose. This issue requires further investigations. The curves reported in figure 1 were obtained with a f value of ~0.2, and a CL yield of ~1.3 $CL \cdot Gy^{-1} \cdot cell^{-1}$. Lower f values (associated to higher CL yields) led to an underestimation of deletions and an overestimation of dicentrics, whereas higher f values (associated to lower CL yields) led to an overestimation of deletions and an underestimation of dicentrics.

Concerning assumption (3), it is based on the fact that, in X-ray-exposed AG1522 human fibroblasts, Cornforth and Bedford [81] observed a one-to-one relationship between the mean number per cell of the so-called "lethal aberrations" (dicentrics, rings and deletions visible in metaphase) and the logarithm of the surviving fraction, which therefore was expressed as:

$$S(D) = e^{-LA(D)} \tag{38}$$

where LA is the mean number of lethal aberrations per cell after a dose D. A similar relationship was observed in V79 Chinese hamster fibroblasts [82]. Although this result cannot be generalized, it is reasonable to assume that it holds also for other cells, basically those cells for which clonogenic inactivation is the main death pathway, whereas other forms of cell death like apoptosis and necrosis do not play an important role. More specifically, the so-called "asymmetrical aberrations" (like dicentrics and centric rings) are capable of forming a "bridge" at anaphase, and in turn the bridge can lead to failure of cytokinesis and thus cell death. On the other hand, an acentric fragment (deletion) either is transmitted (as a paired structure) to one of the two daughter cells, or is not transmitted at all, thus leading to loss of genetic material in the cell progeny; such loss probably plays a small role for cell death in the generation immediately following the loss, but death caused by loss of acentric fragment(s) becomes more important in subsequent generations [82]. These findings explain why dicentrics, centric rings, and (excess) acentric fragments (at least, those fragments that are large enough to cause a significant loss of genetic material [81]), have a high probability of leading to clonogenic cell death, as observed e.g. by Cornforth and Bedford [81]. Of course cell death can also derive from other pathways than (asymmetrical) chromosome aberrations, such as apoptosis, necrosis, etc. As a consequence, the current version of our model is specific for cell types in which cell death via apoptosis and/or necrosis does not play an important role, as is the case of AG1522 and V79 normal cells and of many tumour cells.

After testing against chromosome aberration data and photon survival data, recently the model was applied to ion cell survival, starting with protons. In particular, experimental survival curves [17] were reproduced for AG01522 normal human cells exposed at different depth positions of a 62-MeV proton beam available at INFN-LNS in Catania, Italy, where ocular melanoma is treated [83]. All simulations were performed adopting the same f value used to calculate chromosome aberrations in AG1522 cells, whereas the CL yield was separately adjusted for each curve. Figure 2 reports simulated survival curves compared with experimental data obtained by Chaudhary et al. [17] at six depth positions along a proton SOBP, corresponding to LET values in the range 1.2–25.9 keV/μm. Despite a tendency to underestimate the experimental survival at high doses, a satisfactory agreement between simulations and data was obtained.

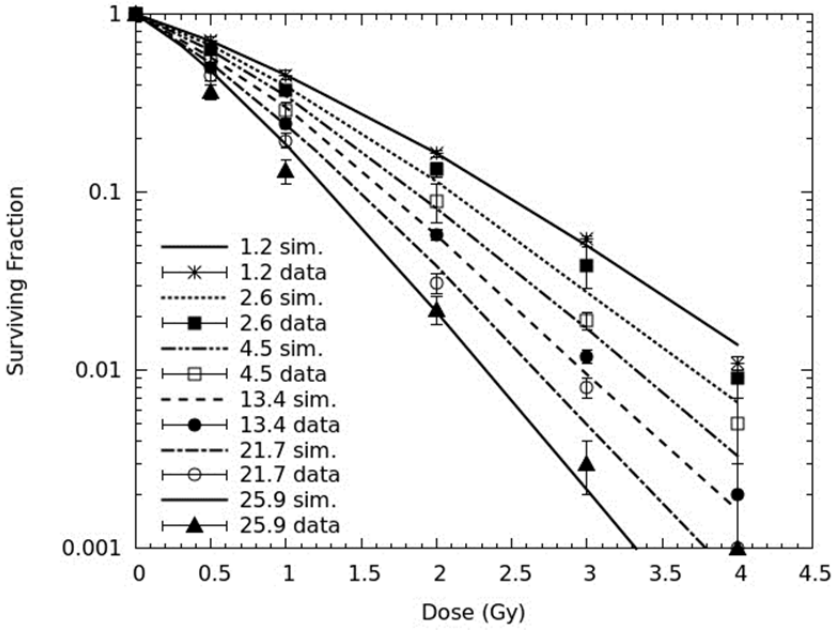

Figure 2. Survival curves for AG01522 normal human fibroblasts irradiated at six depth positions along a proton SOBP available at INFN-LNS, Italy. The various depths correspond to the following dose-averaged LET values: 1.2, 2.6, 4.5, 13.4, 21.7 and 25.9 keV/μm. The lines are simulation outcomes, the points are experimental data taken from [17]. Figure taken from [71].

While for the depth positions considered in the experimental work the cell killing calculations did not add substantial information with respect to the experimental data, the model allowed for full prediction of cell survival also for positions not considered in the experiments, with focus on the dose fall-off region that can be critical for normal tissue damage. Moreover, the model also predicted yields of chromosome aberrations, which were not investigated in the experimental work and may be useful for normal tissue damage evaluation, since there may be a link between chromosome aberrations in normal cells and second tumours [84]. In line with the experimental data reported in [17] and with many other works available in the literature, the beam effectiveness—both for cell death and for chromosome aberrations - was found to increase with depth along the SOBP plateau, and high levels of biological damage were found also beyond the distal dose fall-off. This is due to proton slowing down, which implies an increase in LET and thus in biological effectiveness. Interestingly, the increase in chromosome aberrations with depth was more pronounced than the increase in cell killing. Predictions of cell death and chromosome aberrations were also performed assuming different plateau doses. Increasing the physical dose from 2 to 4 Gy reduced the increase in biological effectiveness along the plateau, whereas decreasing the dose from 2 to 1 Gy led to an even more pronounced increase in effectiveness. This is consistent with the well known dose-dependence of RBE, which tends to be higher at lower doses and *vice-versa*. However, while for cell death the highest considered dose (4 Gy) led to an almost flat biological effectiveness along the plateau, for chromosome aberrations even that dose implied an increase in effectiveness.

The model was also applied to V79 cells, which are rather radio-resistant and have been widely used to characterize many hadrontherapy beams. First, experimental survival curves obtained by

different mono-energetic beams [49,51] were successfully reproduced, adjusting the CL yield for each energy. For a given LET, the CL yields adjusted for V79 cells were lower than those for AG01522, reflecting the lower radio-sensitivity of V79 cells. In fact, as mentioned above, although the CL yield mainly depends on radiation quality, it is also modulated by the specific target cell features. Figure 3 reports calculated survival curves for four monoenergetic proton beams (with LET values in the range 7.7–27.6 keV/μm), as well as X-rays as a reference radiation; the points represent experimental data taken from [49,51]. The X-ray curve was obtained using a CL yield of 1.5 $CL \cdot Gy^{-1} \cdot cell^{-1}$, whereas the four proton curves were obtained with CL yields in the range ~2.0–3.2 $CL \cdot Gy^{-1} \cdot cell^{-1}$, increasing with LET. With these values, the general agreement between the simulation outcomes and the experimental data was satisfactory.

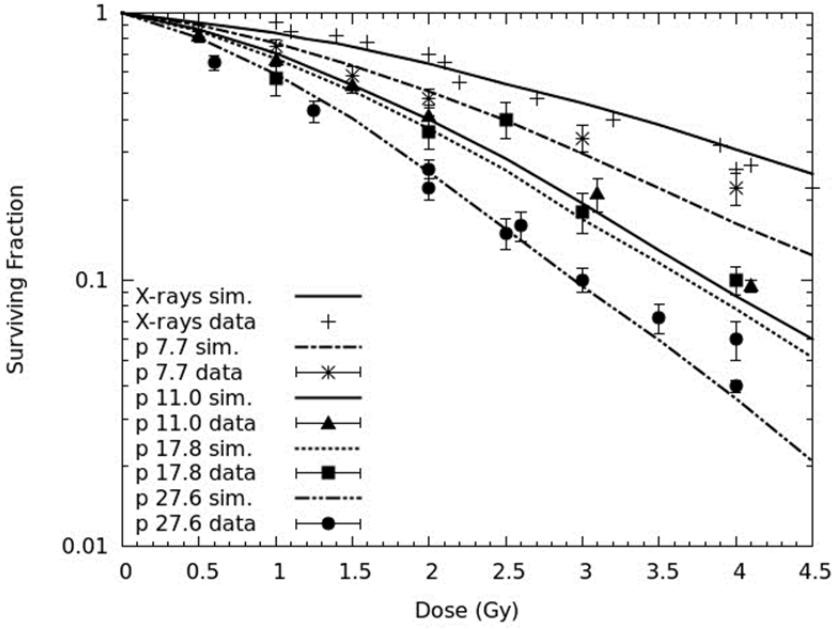

Figure 3. Survival curves for V79 Chinese Hamster fibroblasts exposed to four mono-energetic proton beams (LET: 7.7, 11.0, 17.8 and 27.6 keV/μm), as well as X-rays as a reference radiation. The lines are simulation outcomes, the points are experimental data taken from the literature: [49] for X-rays, 7.7 keV/μm protons and 11.0 keV/μm protons; [51] for X-rays, 17.8 keV/μm protons and 27.6 keV/μm protons. Figure taken from [71].

Afterwards, full predictions of cell death and chromosome aberrations for V79 cells exposed to the Catania hadrontherapy beam were performed. Analogous to AG01522 cells, the beam effectiveness was found to increase along the SOBP plateau, and high levels of biological damage were also found beyond the distal dose fall-off. However, the increase in biological effectiveness was more pronounced for V79 cells than for AG01522 cells. This is consistent with the higher RBE generally shown by cells exhibiting smaller α/β ratios [16], which is the case of V79 cells.

The application of the model to other ions, including carbon, is in progress. Preliminary results on V79 cells irradiated at different depth positions of a Carbon SOBP at the CNAO hadrontherapy centre in Pavia are encouraging. This approach represents a starting point for possible future works

in which treatment plan optimization may be directly based on the calculated level of biological effect. To be of practical use, of course the model needs to be interfaced to a TPS and/or a radiation transport code; to this aim, a collaboration has recently started to develop an interface with the FLUKA code [8] within the MC-INFN project funded by the Italian National Institute of Nuclear Physics. Moreover, the model should be further refined and tested for other cell lines and radiation qualities.

7. Conclusions

Some approaches adopted to evaluate the biological effectiveness of proton and Carbon ions were reviewed. Far from being exhaustive, this review has the main aim of summarizing and discussing the main aspects of the various approaches, also outlining similarities and differences. When possible, the application of these approaches in cancer therapy was also discussed. In addition to the well-known approaches used for Carbon, some examples of biophysical models specifically developed for protons were presented, as well as a model of cell death and chromosome aberrations developed in Pavia. In particular, the analysis concerning protons outlined that, although adopting a constant RBE = 1.1 still seems a reasonable choice, further studies aimed at increasing the accuracy of RBE evaluation in proton therapy are desirable with the final objective of implementing biological models in proton therapy treatment planning, as also suggested by others [85]. Comparing the various approaches to choose the model(s) to be implemented in TPS is not trivial, because the differences in the results are related not only to the approach adopted for modelling the particle biological effectiveness, but also to the physics models underlying the simulation of the various particle interactions in matter. To perform such comparisons, it is therefore desirable that different radiobiological models are implemented in the same radiation transport code.

Acknowledgements

This work was partially supported by the Italian National Institute of Nuclear Physics (INFN), under the projects “ETHICS” and MC-INFN/FLUKA. The authors are also grateful to the Reviewers for their valuable comments.

Conflict of Interest

All authors declare no conflicts of interest in this paper

References

1. Durante M, Loeffler JS (2010) Charged particles in radiation oncology. *Nat Rev Clin Oncol* 7: 37–43.
2. Particle Therapy Co-Operative Group (PTCOG). Available from: http://www.ptcog.ch.
3. Tommasino F, Scifoni E, Durante M (2015) New ions for therapy. *Int J Particle Ther* 2: 428–438.

4. Weyrather WK (2004) Medical Applications of Accelerated Ions, In: Al-Khalili J, Roeckl E, *The Euroschool Lectures on Physics with Exotic Beams,* Berlin, Heidelberg: Springer Berlin Heidelberg, 469–490.
5. Molière G (1948) Theorie der streuung schneller geladener teilchen ii mehrfach-und vielfachstreuung. *Z Naturforschung A* 3: 78–97.
6. Amaldi U, Kraft G (2005) Radiotherapy with beams of carbon ions. *Rep Prog Phys* 68: 1861–1882.
7. Linz U (2012) Physical and biological rationale for using ions in therapy, In: *Ion Beam Therapy,* Berlin, Heidelberg: Springer Berlin Heidelberg, 45–59.
8. Battistoni G, Bauer J, Boehlen TT, et al. (2016) The FLUKA code: An accurate simulation tool for particle therapy. *Front Oncol* 6: 116.
9. Sato T, Niita K, Matsuda N, et al. (2014) Overview of the PHITS code and its application to medical physics. *Prog Nucl Sci Technol* 4: 879–882.
10. Allison J, Amaco K, Apostolakis J, et al. (2016) Recent developments in Geant4. *Nucl Instrum Meth A* 835: 186–225.
11. Scholz M, Kraft G (1994) Calculation of heavy ion inactivation probabilities based on track structure, X ray sensitivity and target size. *Radiat Prot Dosim* 52: 29–33.
12. Kase Y, Kanai T, Matsumoto Y, et al. (2006) Microdosimetric measurements and estimation of human cell survival for heavy-ion beams. *Radiat Res* 166: 629–638.
13. Wouters BG, Lam GK, Oelfke U, et al. (1996) Measurements of relative biological effectiveness of the 70 MeV proton beam at TRIUMF using V79 cells and the high precision cell sorter assay. *Radiat Res* 146: 159–170.
14. Gerweck LE, Kozin SV (1999) Relative biological effectiveness of proton beams in clinical therapy. *Radiother Oncol* 50: 135–142.
15. Paganetti H (2002) Relative Biological Effectiveness (RBE) values for proton beam therapy. *J Radiat Oncol Biol Phys* 53: 407–421.
16. Paganetti H, van Luijk P (2013) Biological considerations when comparing proton therapy and photon therapy. *Semin Radiat Oncol* 23: 77–87.
17. Chaudary P, Marshall TI, Perozziello FM, et al. (2014) Relative biological effectiveness variation along monoenergetic and modulated bragg peaks of a 62-MeV therapeutic proton beam: a preclinical assessment. *Int J Radiat Oncol Biol Phys* 90: 27–35.
18. Michaelidesová A, Vachelová J, Puchalska M, et al. (2017) Relative biological effectiveness in a proton spread-out Bragg peak formed by pencil beam scanning mode. *Australas Phys Eng Sci Med* 40: 359–368.
19. Grün R, Friedrich T, Krämer M, et al. (2017) Systematics of relative biological effectiveness measurements for proton radiation along the spread out Bragg peak: experimental validation of the local effect model. *Phys Med Biol* 62: 890–908.
20. Scholz M, Kraft G (1996) Track structure and the calculation of biological effects of heavy charged particles. *Adv Space Res* 18: 5–14.
21. Hubert F, Fleury A, Bimbot R, et al. (1980) Range and stopping power tables for 2.5–100 MeV/nucleon heavy ions in solids. *Ann Phys* 5: 214–218.
22. Nortllcliff LC, Shilling RF (1970) Range and stopping power tables for heavy ions. *Atom Data Nucl Data* 7: 233–437.

23. Elsässer T, Krämer M, Scholz M (2008) Accuracy of the local effect model for the prediction of biologic effects of carbon ion beams in vitro and in vivo. *Int J Radiat Oncol Biol Phys* 71: 866–872.
24. Kiefer J, Straaten H (1986) A model of ion track structure based on classical collision dynamics. *Phys Med Biol* 31: 1201–1209.
25. Scholz M, Kellerer AM, Kraft-Weyrather W, et al. (1997) Computation of cell survival in heavy ion beams for therapy. The model and its approximation. *Radiat Environ Bioph* 36: 59–66.
26. Elsässer T, Scholz M (2007) Cluster effects within the local effect model. *Radiat Res* 167: 319–329.
27. Elsässer T, Weyrather WK, Friedrich T, et al. (2010) Quantification of the relative biological effectiveness for ion beam radiotherapy: direct experimental comparison of proton and carbon ion beams and a novel approach for treatment planning. *Int J Radiat Oncol Biol Phys* 78: 1177–1183.
28. Grün R, Friedrich T, Elsässer T, et al. (2012) Impact of enhancements in the Local Effect Model (LEM) on the predicted RBE-weighted target dose distribution in carbon ion therapy. *Phys Med Biol* 57: 7261–7274.
29. Kanai T, Furusawa Y, Fukutsu K, et al. (1997) Irradiation of mixed beam and design of spread-out Bragg peak for heavy-ion radiotherapy. *Radiat Res* 147: 78–85.
30. Kanai T, Endo M, Minohara S, et al (1999) Biophysical characteristics of HIMAC clinical irradiation system for heavy-ion radiation therapy. *Int J Radiat Oncol Biol Phys* 44: 201–210.
31. Kraft G (2002) Radiobiological effecs of highly-charged ions, In: Currel FJ, *The physics of highly and multiply charged ions,* Kluwer Academic Publisher.
32. Mizoe J, Tsujii H, Kamada T, et al. (2004) Dose escalation study of carbon ion radiotherapy for locally advanced head-and-neck cancer. *Int J Radiat Oncol Biol Phys* 60: 358–364.
33. Kanai T, Matsufuji N, Miyamoto T, et al. (2006) Examination of GyE system for HIMAC carbon therapy. *Int J Radiat Oncol Biol Phys* 64: 650–656.
34. Hawkins RB (1994) A statistical theory of cell killing by radiation of varying linear energy transfer. *Radiat Res* 140: 366–374.
35. Hawkins RB (2003) A microdosimetric-kinetic model for the effect of non-Poisson distribution of lethal lesions on the variation of RBE with LET. *Radiat Res* 160: 61–69.
36. Kellerer M, Rossi HH (1978) A generalized formulation of dual radiation action. *Radiat Res* 75: 471–488.
37. Kase Y, Kanai T, Matsufuji N, et al. (2008) Biophysical calculation of cell survival probabilities using amorphous track structure models for heavy-ion irradiation. *Phys Med Biol* 53: 37–59.
38. Inaniwa T, Furukawa T, Kase Y, et al. (2010) Treatment planning for a scanned carbon beam with a modified microdosimetric kinetic model. *Phys Med Biol* 55: 6721–6737.
39. Furusawa Y, Fukutsu K, Aoki M, et al. (2000) Inactivation of aerobic and hypoxic cells from three different cell lines by accelerated He-, C- and Ne-ion beams. *Radiat Res* 154: 485–496.
40. Inaniwa T, Furukawa T, Sato S, et al. (2008) Development of treatment planning for scanning irradiation at HIMAC. *Nucl Instr Meth Phys Res B* 266: 2194–2198.
41. Sato T, Kase Y, Watanabe R, et al. (2009) Biological dose estimation for charged particle therapy using an improved PHITS code coupled with a MK model. *Radiat Res* 171: 107–117.
42. Sato T, Furusawa Y (2012) Cell survival fraction estimation based on the probability densities of domain and cell nucleus specific energies using improved Microdosimetric Kinetic Models. *Radiat Res* 178: 341–356.

43. Sato T, Hamada N (2014) Model assembly for estimating cell surviving fraction for both targeted and nontargeted effects based on microdosimetric probability densities. *PloS One* 9: e114056.
44. Kramer M, Wang JF, Weyrather W (2003) Biological dosimetry of complex ion radiation fields. *Phys Med Biol* 48: 2063–2070.
45. Magro G, Dahle TJ, Molinelli S, et al. (2017) The FLUKA Monte Carlo code coupled with the NIRS approach for clinical dose calculations in carbon ion therapy. *Phys Med Biol* 62: 3814–3827.
46. Frese MC, Yu VK, Stewart RD, et al. (2012) A mechanism-based approach to predict the relative biological effectiveness of protons and carbon ions in radiation therapy. *Int J Radiat Oncol Biol Phys* 83: 442–450.
47. Tilly N, Johansson J, Isacsson U, et al. (2005) The influence of RBE variations in clinical proton treatment plan for a hypopharynx cancer. *Phys Med Biol* 50: 2765–2777.
48. Belli M, Cera F, Cherubini R, et al. (1993) Inactivation and mutation induction in V79 cells by low energy protons: re-evaluation of the results at the LNL facility. *Int J Radiat Biol* 63: 331–337.
49. Belli M, Cera F, Cherubini R, et al. (1998) RBE-LET relationships for cell inactivation and mutation induced by low energy protons in V79 cells: further results at the LNL facility. *Int J Radiat Biol* 74: 501–509.
50. Belli M, Bettega D, Calzolari P, et al. (2000) Inactivation of human normal and tumour cells irradiated with low energy protons. *Int J Radiat Biol* 76: 831–839.
51. Folkard M, Prise KM, Vojnovic B, et al. (1996) Inactivation of V79 cells by low-energy protons, deuterons and helium-3 ions. *Int J Radiat Biol* 69: 729–738.
52. Bettega D, Calzolari P, Marchesini R, et al. (1998) Inactivation of C3H10T1/2 cells by low energy protons and deuterons. *Int J Radiat Biol* 73: 303–309.
53. Frese MC, Wilkens JJ, Huber PE, et al. (2011) Application of constant vs. variable relative biological effectiveness in treatment planning of intensity-modulated proton therapy. *Int J Radiat Oncol Biol Phys* 79: 80–88.
54. Wilkens JJ, Oelfke U (2004) A phenomenological model for the relative biological effectiveness in therapeutic proton beams. *Phys Med Biol* 49: 2811–2825.
55. ICRU (1993) Stopping powers and ranges for protons and alpha particles, report 49, International Commission on Radiation Units and Measurements, Bethesda, MD, USA.
56. Carabe-Fernandez A, Moteabbed M, Depauw N, et al. (2012) Range uncertainty in proton therapy due to variable biological effectiveness. *Phys Med Biol* 57: 1159–1172.
57. Belli M, Cherubini R, Finotto S, et al. (1989) RBE-LET relationship for the survival of V79 cells irradiated with low energy protons. *Int J Radiat Biol* 55: 93–104.
58. Perris A, Pialoglou P, Katsanos AA, et al. (1986) Biological effectiveness of low energy protons. I. Survival of chinese hamster cells. *Int J Radiat Biol* 50: 1093–1101.
59. Coutrakon G, Cortese J, Ghebremedhin A, et al. (1997) Microdosimetry spectra of the Loma Linda proton beam and relative biological effectiveness comparisons. *Med Phys* 24: 1499–1506.
60. Wedenberg M, Lind BK, Hardemark B (2013) A model for the relative biological effectiveness of protons: the tissue specific parameter α/β of photons is a predictor for the sensitivity to LET changes. *Acta Oncol* 52: 580–588.

61. Paganetti H (2014) Relative biological effectiveness (RBE) values for proton beam therapy. Variations as a function of biological endpoint, dose, and linear energy transfer. *Phys Med Biol* 59: R419–R472.
62. McNamara AL, Schuemann J, Paganetti H (2015) A phenomenological relative biological effectiveness (RBE) model for proton therapy based on all published in vitro cell survival data. *Phys Med Biol* 60: 8399–8416.
63. Wedenberg M, Toma-Dasu I (2014) Disregarding RBE variation in treatment plan comparison may lead to bias in favor of proton plans. *Med Phys* 41: 091706.
64. Giovannini G, Böhlen T, Cabal G, et al. (2016) Variable RBE in proton therapy: comparison of different model predictions and their influence on clinical-like scenarios. *Radiat Oncol* 11: 68.
65. Ottolenghi A, Ballarini F, Biaggi M (2001) Modelling chromosomal aberration induction by ionising radiation: the influence of interphase chromosome architecture. *Adv Space Res* 27: 369–382.
66. Ballarini F, Ottolenghi A (2004) A model of chromosome aberration induction and CML incidence at low doses. *Radiat Environ Bioph* 43: 165–171.
67. Ballarini F (2010) From DNA radiation damage to cell death: Theoretical approaches. *J Nucleic Acids*.
68. Ballarini F, Altieri S, Bortolussi S, et al. (2013) A model of radiation-induced cell killing: insights into mechanisms and applications for hadrontherapy. *Radiat Res* 180: 307–315.
69. Ballarini F, Altieri S, Bortolussi S, et al. (2014) The BIANCA model/code of radiation-induced cell death: application to human cells exposed to different radiation types. *Radiat Environ Bioph* 53: 525–533.
70. Carante MP, Altieri S, Bortolussi S, at al. (2015) Modelling radiation-induced cell death: role of different levels of DNA damage clustering. *Radiat Environ Bioph* 54: 305–316.
71. Carante MP, Ballarini F (2016) Calculating variations in biological effectiveness for a 62 MeV proton beam. *Front Oncol* 6: 76.
72. Ballarini F, Carante MP (2016) Chromosome aberrations and cell death by ionizing radiation: evolution of a biophysical model. *Radiat Phys Chem* 128C: 18–25.
73. Aiginger HV, Andersen F, Ballarini, et al. (2005) The FLUKA code: new developments and application to 1 GeV/n Iron beams. *Adv Space Res* 35: 214–222.
74. Ballarini F, Ottolenghi A (2005) A model of chromosome aberration induction: applications to space research. *Radiat Res* 164: 567–570.
75. Ballarini F, Alloni D, Facoetti A, et al. (2007) Radiation risk estimation: modelling approaches for "targeted" and "non-targeted" effects. *Adv Space Res* 40: 1392–1400.
76. Campa AD, Alloni F, Antonelli, et al. (2009) DNA fragmentation induced in human fibroblasts by 56Fe ions: experimental data and MC simulations. *Radiat Res* 171: 438–445.
77. Wu H, George K, Yang TC (1999) Estimate of the frequency of true incomplete exchanges in human lymphocytes exposed to 1 GeV/u Fe ions in vitro. *Int J Radiat Biol* 75: 593–599.
78. Cornforth MN, Bedford JS (1985) On the nature of a defect in cells from individuals with Ataxia-Telangiectasia. *Science* 227: 1589–1591.
79. Boei JJ, Vermeulen S, Mullenders LH, et al. (2001) Impact of radiation quality on the spectrum of induced chromosome exchange aberrations. *Int J Radiat Biol* 77: 847–857.

80. Chen AM, Lucas JN, Simpson PJS, et al. (1997) Computer simulation of data on chromosome aberrations produced by X rays or alpha particles and detected by fluorescence in situ hybridization. *Radiat Res* 148: S93–S101.
81. Cornforth M, Bedford J (1987) A quantitative comparison of potentially lethal damage repair and the rejoining of interphase chromosome breaks in low passage normal human fibroblasts. *Radiat Res* 111: 385–405.
82. Carrano AV (1973) Chromosome aberrations and radiation-induced cell death. I. Transmission and survival parameters of aberrations. *Mutat Res* 17: 341–353.
83. Cuttone G, Cirrone GAP, Di FG, et al. (2011) CATANA protontherapy facility: The state of art of clinical and dosimetric experience. *Eur Phys J Plus* 126: 65.
84. Rabbits T (1994) Chromosomal translocations in human cancer. *Nature* 372: 143–149.
85. Tommasino F, Durante M (2015) Proton radiobiology. *Cancers* 7: 353–381.

AIMS Press